INSTITUTE OF PHYSICS PUBLISHING and INTERNATIONAL ATOMIC ENERGY AGENCY NUCLEAR FUSION
Nucl. Fusion **45** (2005) 264–270 doi:10.1088/0029-5515/45/4/007

Observation of a high performance operating regime with small edge-localized modes in the National Spherical Torus Experiment

R. Maingi[1], K. Tritz[2], E.D. Fredrickson[3], J.E. Menard[3], S.A. Sabbagh[4], D. Stutman[2], M.G. Bell[3], R.E. Bell[3], C.E. Bush[1], D.A. Gates[3], D.W. Johnson[3], R. Kaita[3], S.M. Kaye[3], H.W. Kugel[3], B.P. LeBlanc[3], D. Mueller[3], R. Raman[5], A.L. Roquemore[3] and V.A. Soukhanovskii[6]

[1] Oak Ridge National Laboratory, Oak Ridge, TN 37831, USA
[2] Physics and Astronomy Department, Johns Hopkins University, Baltimore, MD, USA
[3] Princeton Plasma Physics Laboratory, PO Box 451, Princeton, NJ 08543, USA
[4] Applied Physics and Math Department, Columbia University, New York, NY, USA
[5] Department of Aeronautics and Astronautics, University of Washington, Seattle, WA, USA
[6] Lawrence Livermore National Laboratory, Livermore, CA, USA

Received 10 September 2004, accepted for publication 23 February 2005
Published 23 March 2005
Online at stacks.iop.org/NF/45/264

Abstract
We report the observation of a high performance scenario in the National Spherical Torus Experiment with very small edge-localized modes (ELMs). These ELMs, individually, have no measurable impact on the stored energy and are observed by several diagnostics. The small ELMs have clear differences as compared with the ELM types reported in the literature, and this operating mode has distinct features compared with other high performance tokamak scenarios with little or no ELMs. The ELM is termed as 'type V', and it has a short-lived $n = 1$ magnetic precursor oscillation rotating counter to the plasma current and a distinct signature on the soft x-ray system. If we could extrapolate it, this scenario would provide an attractive operating regime for next step fusion experiments.

(Some figures in this article are in colour only in the electronic version)

PACS numbers: 52.55.Fa, 52.55.Rk

1. Introduction

The search for high performance operating regimes with few or no edge-localized modes (ELMs) has been a high priority in nuclear fusion research. The baseline operating scenario for the International Thermonuclear Experimental Reactor (ITER) relies on H-mode confinement and profiles [1]. In most H-mode discharges in conventional aspect ratio tokamaks, ELMs are observed, which serve to flush fuel and impurity particles from the edge plasma into the Scrape-Off-Layer and divertor plasma. This periodic edge ejection results in transiently high power and particle loads to the plasma facing components (PFCs). The best plasma performance is often realized in the type I ELM regime (which is ITER's baseline scenario), but the type I ELM typically results in larger heat pulses than other ELM types [2]. Such transient PFC loading is tolerable in present day machines, but extrapolations show severe PFC damage resulting in larger, higher power density machines (such as ITER) when the ELM power loading exceeds material dependent limits [3].

Several high performance regimes either without ELMs or with few ELMs have been identified in conventional aspect ratio tokamaks. The quiescent H-mode (QH-mode) is a high performance, largely ELM-free regime discovered [4] on the DIII-D tokamak and recently reproduced in other devices. The QH-mode scenario requires neutral beam injection (NBI) counter to the direction of plasma current (I_p), low density, and relies on the presence of an edge harmonic oscillation for particle control. The enhanced D_α (EDA) H-mode has been identified by the Alcator C-MOD group, and it relies on a quasi-coherent MHD mode in the vicinity of the separatrix for particle control [5]. The EDA H-mode bears

strong resemblance to the earlier PDX forced density rise scenario, another high performance scenario with small/no ELMs [6], and the more recent high recycling steady (HRS) H-mode in JFT-2M [7]. Access to small ELMs was also reported at high triangularity [8] or poloidal beta (β_p) [9] in JT-60U. We note also the recent success in generating high performance discharges with no/few large ELMs using a stochastic boundary layer in DIII-D, which also provided good density control [10]. The operating regime achieved in the National Spherical Torus Experiment (NSTX) and reported here is distinct from all of these: (1) there is no counter injection or edge harmonic oscillation as in the QH-mode; (2) there is no quasi-coherent mode in the edge plasma as in EDA or related H-mode scenarios; (3) the β_p threshold needed to access this small ELM regime is $\geqslant$0.6 and no enhanced plasma shaping was required; and (4) no stochastic boundary technique was used to suppress ELMs. In addition, the ELM characteristics and precursors appear significantly different from existing ELM types in the literature and other ELM types observed in NSTX. Hence, this regime provides another small ELM regime for possible use in large fusion devices to provide density control without the significant heat flux transients associated with conventional type I ELMs and without the performance degradation observed in type III ELMs [11] (i.e. no degradation comparing type I and the small ELM discharges in NSTX). We refer to the perturbations in NSTX as type V ELMs (note that a low density branch [12] of the traditionally high density type III ELMs was observed in DIII-D and is sometimes referred to as a type IV ELM in the community), and emphasize that the use of a new number is based on the measured characteristics. Detailed stability calculations may prove, however, similarity between the underlying instabilities.

2. Description of high performance regime

The NSTX is a medium-sized, low aspect ratio spherical tokamak [13] with the following parameters: major radius $R = 0.85$ m, minor radius $a = 0.67$ m, $R/a \geqslant 1.26$, toroidal field $B_t \leqslant 0.6$ T, with up to 7 MW of NBI power (P_{NBI}) and 6 MW of radio-frequency heating. The basic characteristics of the NSTX high performance, small ELM regime are shown in figure 1 for a lower-single null diverted discharge with $I_p = 0.8$ MA, $B_t = 0.5$ T, $P_{NBI} = 4.1$ MW, and the following parameters evaluated at the separatrix: elongation $\kappa \sim 1.9$, lower triangularity $\delta_L \sim 0.5$ and upper triangularity $\delta_U \sim 0.3$. The line-average density continuously rises after the H-mode transition at $t = 230$ ms (figure 1(b)). Type V ELMs with a frequency ~400 Hz can be observed on the lower divertor D_α starting at $t \sim 340$ ms, although a few irregularly spaced type V ELMs are observed near 290 and 320 ms. Gas puffing from the centre stack lasts throughout the discharge (figure 1(c)); the combination of this fuelling and the NBI particle source contribute to the observed density rise. The stored energy remains flat for about 370 ms or ~7 energy confinement times (τ_E), and the confinement enhancement over ITER-97L scaling [14] is steady at ~2.2. For reference, the steady β_p was ~1.2 (bootstrap current fraction 40–50%) and the line-averaged density relative to Greenwald scaling [15] ($n_{GW} = I_p/\pi a^2$) was 0.85 just before the end of the discharge, which was terminated by I_p ramp-down.

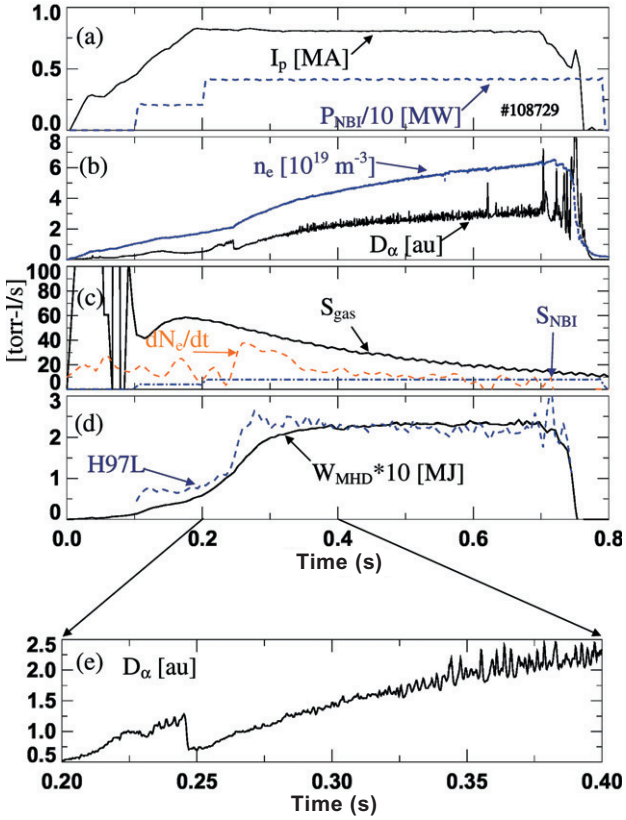

Figure 1. High performance discharge with type V ELMs: (a) I_p and P_{NBI}, (b) lower divertor D_α emission and line-averaged density ($\overline{n_e}$), (c) NBI (S_{NBI}) and gas (S_{gas}) fuelling rates, and density rise rate (dN_e/dt) and (d) stored energy (W_{MHD}) and energy confinement normalized to the ITER-97L scaling. The D_α emission time base is expanded in frame (e).

We note that details of this high performance regime for similar discharges have been reported previously [16–20]. The new interpretation presented in this paper pertains to (1) the positive identification of the D_α oscillations as tiny ELMs, which are different from ELMs in the published literature, and (2) the recent observation of conventional intermediate-sized ELMs (which have characteristics of both type II and III) in NSTX which confirm the uniqueness of these type V ELMs. For completeness, we note that recent overviews of NSTX results [21] and ELM/pedestal studies [22] provide more detailed reference material.

3. ELM characteristics

Many ELM types, including type I, II/III and the new type V, have been observed [23] in NSTX. Figure 2 contrasts the characteristics of these ELM types. The stored energy fractional drop (computed from reconstructions with the EFITD code [24] applied to NSTX [25] with a 0.25 ms time resolution) is typically between 5–15%, 1–4% and $\leqslant$1% for type I, II/III and V ELMs, respectively. There is some ambiguity in identifying the ELM type in the middle column: these ELMs were observed with heating power starting close to but extending well above the L–H power threshold (i.e. some similarity to type III) [11] in a shape very close to or just at a balanced double-null (i.e. similar to type II) [26, 27].

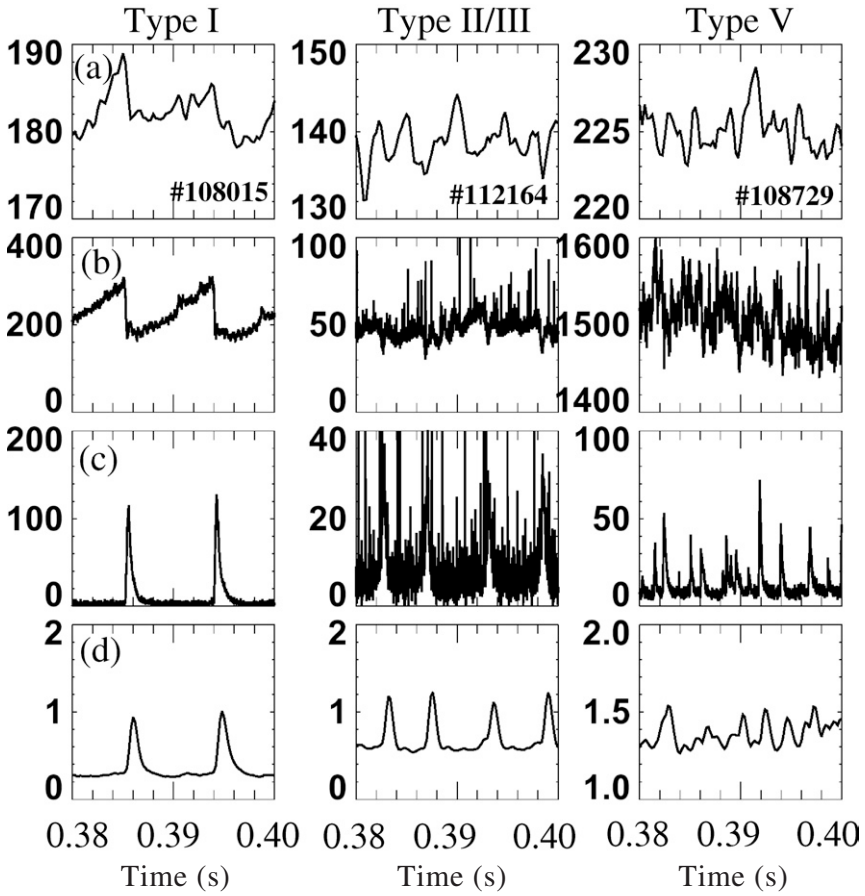

Figure 2. Characteristics of different ELM types in NSTX: (*a*) W_{MHD}, (*b*) USXR chord inside of the inversion radius, (*c*) USXR chord outside of the inversion radius and (*d*) lower divertor D_α emission. The USXR data were obtained with a 5 μm thick Be filter.

The frequency of the type II/III ELMs decreased with heating power and increased with density, with the latter presumably caused by the increased radiated power and consequent reduced loss power through the edge plasma as the density increased.

Each of the ELM types discussed above can also be observed in the ultra soft x-ray (USXR) data [28] in panels (*b*) and (*c*) of figure 2. We note that the USXR emission with the 5 μm Be filter scales approximately with the edge parameters as $n^2_{e,edge}T^{0.5}_{e,edge}$. In comparison, the core USXR emission with the 100 μm Be filter scales more strongly with the core electron temperature. There is an inversion layer in the edge USXR channels; inside of the inversion layer, i.e. panels 2(*b*), the emission drops, consistent with an outflow of particles and energy from the area. Outside the inversion layer, i.e. panels 2(*c*), an increase in the emission is observed.

The type V ELMs increased the outer divertor D_α profile (figure 3) by ∼30–50%, and the inner divertor profile by only ∼10–15%. Note that these ELMs were not the result of a long-lived coherent MHD mode. Low-*n* intermediate frequency (20–40 kHz) coherent modes (figure 4) were observed in the core from 300 to 700 ms, but these modes began just after the type V ELM activity. The radial location of the mode was determined through inspection of the USXR data. In other discharges it was observed that these coherent modes persisted even after the ELMs stopped. Thus, it is unlikely that the core modes are the source of the ELMs.

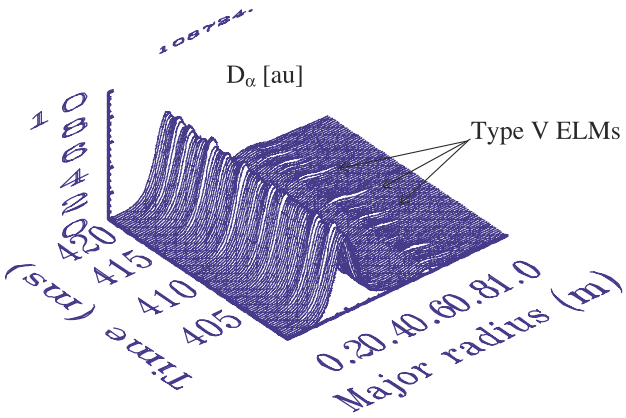

Figure 3. ELMs observed as small perturbations on divertor D_α radial profile, with a larger impact on the outboard side than the inboard side.

Insight into the ELM size, affected spatial depth and spatial origin can be obtained through examination of the USXR profile data [28]. At the time of these experiments, three arrays were implemented on NSTX: one each looking into the lower and upper divertors, and one looking from the top across the entire poloidal cross-section (figure 5). The chords are spaced approximately 3 cm apart, and 5 μm Be foil filters were used to focus on emission from the edge of the plasma for the lower divertor and vertical arrays, whereas the

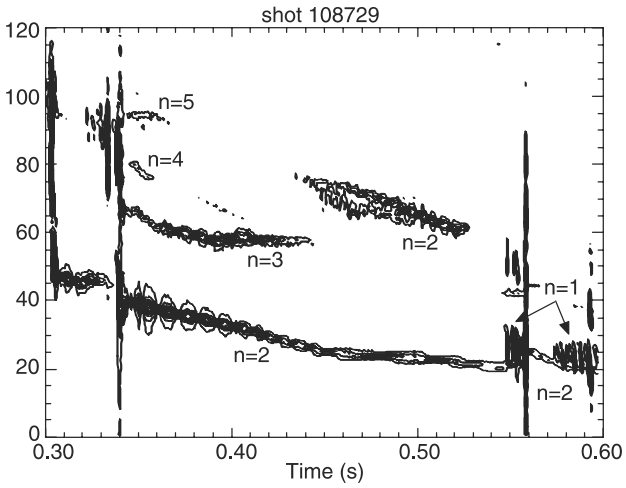

Figure 4. Spectrum of instabilities with $n = 1$–6 for #108729: coherent MHD activity in the core plasma begins at about 0.3 s and persists during the type V ELM phase. The $n = 1$ modes are 'chirping modes', i.e. changing in frequency. Data are plotted from the blue Mirnov sensors (just above the outer midplane) in figure 5.

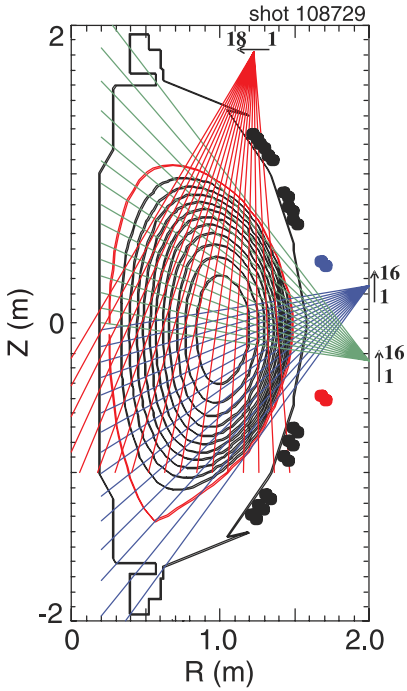

Figure 5. USXR view geometry of three arrays for #108729 at 0.35 s. The locations of the poloidal Mirnov sensors are indicated by black squares, and two sensors from the toroidal arrays are indicated by red and blue squares.

upper divertor array had a 100 μm Be foil filter to focus on core USXR emission. The data were sampled at 190 kHz. For the vertical array, the chord numbering starts at 1 for the chord nearest the outer midplane and increases to 18 for the chord nearest the inner midplane. For the lower divertor array, the chord numbering starts at 1 for the lowest chord and increases to 16 for the chord near the midplane. A thick filter was used on the upper divertor array to verify that these ELMs did not extend into the core. The radial extent of the USXR perturbation during the ELM was limited to a few chords. Because the USXR data are line-averaged, this observation indicates that the perturbation is in a very narrow region near the pedestal.

Figure 6(a) shows a contrast enhanced contour plot of two type V ELMs in the vertical USXR array data from the discharge in figure 1. Note that the oscillation (e.g. the event starting near $t = 0.4123$ s) first appears on ~chord 6, and propagates to chord 1 and then disappears for several tens of microseconds. Figure 6(b) shows the same events on the lower divertor array. In the time the perturbation disappears from the view of the vertical array, it appears in ~chord 5 of the lower divertor array and then propagates rapidly to chord 16. Shortly after disappearing from the lower divertor array, the ELM reappears in chord 1 of the vertical array and propagates to chord 6 before dissipating. The geometry of the vertical array misses the plasma at the outer midplane. Hence, the disappearance of the ELM on the data from that array signifies propagation to the outer midplane at that time. Simple triangulation indicates that the ELM is first observed in the lower divertor region at the toroidal location of the USXR arrays, possibly in the vicinity of the X-point, and then propagates with a poloidal component to the outer midplane and then back around to the top of the machine. The duration of this perturbation on the USXR is ~200–500 μs, and the USXR perturbation precedes the divertor D_α light enhancement by several hundred microseconds, indicating that the diagnostics indeed observe the same perturbation; the USXR data on the closed field lines and then the divertor D_α after the perturbation crosses the separatrix to open field lines.

Near the onset of the perturbation in the USXR, a rotating mode with toroidal mode number $n = 1$ is observed in the toroidal and poloidal Mirnov arrays below the outer midplane, as shown from a different discharge with a type V ELM in figure 7. This mode persists for about two toroidal transit times before the type V ELM crash and propagates in the counter I_p direction. In comparison, higher-n modes are sometimes observed for 200–300 μs prior to type I ELM crashes, and coherent mode activity is observed for up to several milliseconds before a type II/III ELM crash [22].

An important parameter in determining whether type II/III ELMs or type V ELMs are obtained is the either the X-point magnetic balance, quantified by the radial distance between the two X-points mapped to the outer midplane, and/or the plasma elongation κ. The former parameter, referred to as δ_r^{sep} in the literature, has been shown to affect not only the ELM type [27], but also the up/down power balance [29], and the L–H power threshold [30]. A comparison of two shapes in NSTX with $\delta_r^{sep} \sim -1.5$ cm (and a modest κ difference of ~5%) is shown in figure 8, and the effect on the ELMs as manifested in divertor D_α emission is shown in figure 9. When δ_r^{sep} lies between 0 and (-1) cm, i.e. biased towards the lower X-point and higher κ, type II/III ELMs are obtained, whereas type V ELMs are obtained at larger δ_r^{sep} values at lower κ. We note that the identification of the ELM type was based on the USXR characteristics, the size of the stored energy drop per ELM, as well as the presence or absence of the long-lived magnetic precursor discussed above.

Originally [26], type II ELMs were proposed to be caused by an improved access to the second stability region, which in turn was caused by the reduced edge magnetic shear associated

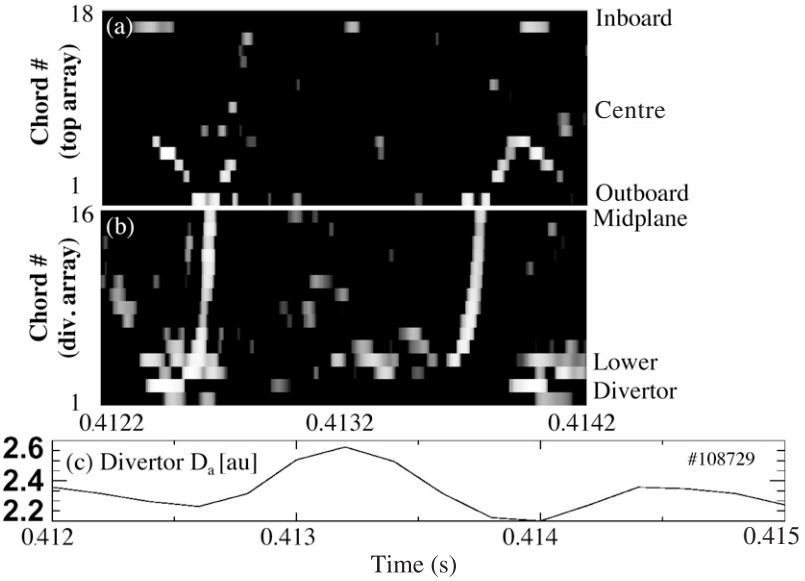

Figure 6. USXR view of type V ELM: (*a*) contour plot of vertical USXR data (red array from figure 5) showing ELM propagation, (*b*) contour plot of lower divertor USXR data (blue array from figure 5) showing ELM propagation and (*c*) divertor D_α emission. The USXR data were obtained with a 5 μm thick Be filter.

with high q_{95} operation from high κ or triangularity δ. Type II ELMs were also observed [27] when $\delta_r^{sep} < 0.5$ cm, which effectively also reduced the edge magnetic shear. Our observations for type V ELMs are exactly the opposite of these previous works: type V ELMs are observed at larger δ_r^{sep}/lower κ, where the magnetic shear is increased, which should tend to restrict access to second stability.

We note that preliminary edge stability calculations for the discharge in figure 1 indicated that the edge plasma began to exceed the ideal high-n ballooning limit starting at $t = 0.29$ s. The spatial region of instability grew gradually larger with time. Temporal correlation with individual type V ELMs was not possible due to the limited time and spatial resolution of edge diagnostics. The equilibrium reconstructions [19] for these stability calculations with the DCON code [31] was based on external magnetic signals and several plasma profiles. Near term improvements to the spatial resolution of edge diagnostics as well as the measurement of the magnetic field line pitch via the motional Stark effect diagnostic will allow a more thorough assessment of the edge stability in these discharge scenarios.

4. Particle control aspects

One critical question is the ability of the type V ELMs to provide sufficient density and impurity control. Experimentally, it is observed that the edge carbon density and radiation increased during these discharges, but the core radiated power and Z_{eff} remained low. Part of the density rise may have been the result of continuous fuelling from the centre stack gas injection system, which has a ~550 ms e-folding on the fuelling rate after activation. The density rise from #108729 was examined via a simple particle balance model:

$$\frac{dN}{dt} = \eta_{NBI} S_{NBI} + \eta_{gas} S_{gas}(t) - \frac{N}{\tau_p^*}. \qquad (1)$$

Here, N is the particle content inside the separatrix, S_{NBI} and $S_{gas}(t)$ are the NBI and gas fuelling rates, η_{NBI} and η_{gas} are the NBI and external gas direct fuelling efficiencies and τ_p^* is the particle containment time. The gas fuelling rate from the centre stack is given by:

$$S_{gas}(t) = S_{gas,0} \exp\left(-\frac{t}{\tau_{gas}}\right); \qquad \tau_{gas} \sim 0.55\,\text{s}. \qquad (2)$$

The density rise ($\Delta N(t)$) following a step change in particle confinement at the L–H transition is obtained analytically by solving equation (1):

$$\Delta N(t) = (\eta_{NBI} S_{NBI} \tau_p^* - N_0)\left(1 - \exp\left(-\frac{t}{\tau_p^*}\right)\right) + \frac{\eta_{gas} S_{gas,0} \tau_{gas} \tau_p^*}{\tau_{gas} - \tau_p^*}\left[\exp\left(-\frac{t}{\tau_{gas}}\right) - \exp\left(-\frac{t}{\tau_p^*}\right)\right]. \qquad (3)$$

Assuming that the fuelling efficiencies do not change appreciably during the density rise, the time dependence of the density can be fit to obtain $\tau_p^* \sim 0.5$ s, yielding a $\tau_p^*/\tau_E \sim 9$. We caution that the solution in equation (3) has a mathematical singularity when τ_p^* approaches τ_{gas}, and that the fitting interval was approximately $1 \times \tau_p^*$, limited by the pulse length. Nonetheless, we note that this value is approximately the same value obtained in DIII-D long pulse H-modes before active divertor pumping was enabled; the DIII-D ratio was reduced by ~50% (by reducing τ_p^*) with efficient in-vessel cryo-pumping (i.e. the line-averaged density was reduced by at least a factor of 2) [32]. We also note that the density rises even more quickly in NSTX ELM-free discharges than in discharges with type V ELMs. Thus, it is probable that NSTX could achieve a similar reduction in τ_p^*/τ_E with an efficient active pumping scheme, implying that the particle confinement reduction provided by these ELMs will allow for sufficient density control.

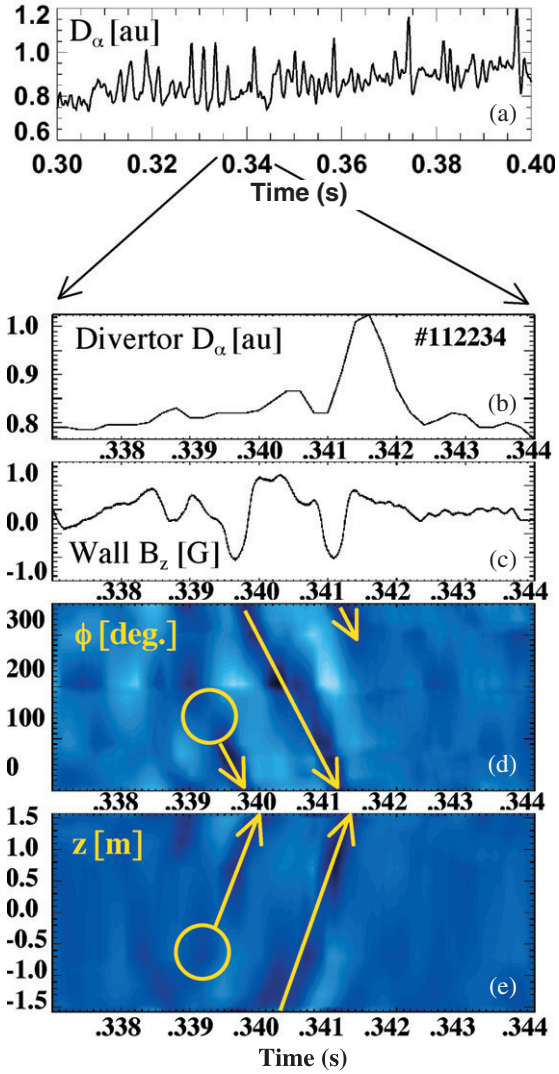

Figure 7. Magnetic signature of type V ELMs: (*a*) divertor D_α, (*b*) expanded scale D_α, (*c*) magnetic perturbation size at wall at $\phi = 30^\circ$, (*d*) toroidal Mirnov array (red sensors from figure 5) with dark blue bands showing mode toroidal propagation counter to I_p and (*e*) passive plate Mirnov array (black sensors from figure 5) with dark blue bands showing mode poloidal propagation upwards. The approximate mode birth is highlighted by circles in (*d*) and (*e*).

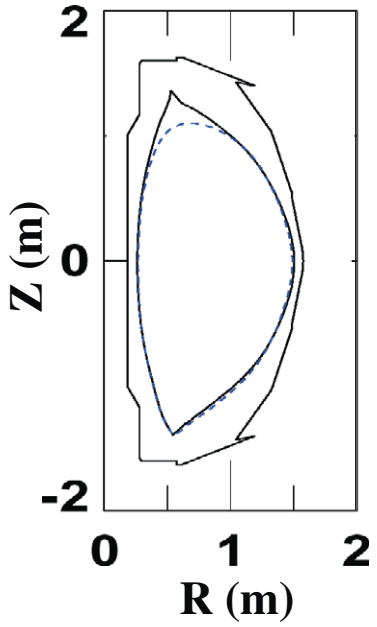

Figure 8. Shape comparison between double-null (DN solid: #112523 at 0.301) and lower-single null (LSN dashed: #112498 at 0.301) with $\delta_r^{sep} = -1.5$ cm. Note also that the plasma elongation κ is ~2.1 in the DN and 2.0 in the LSN.

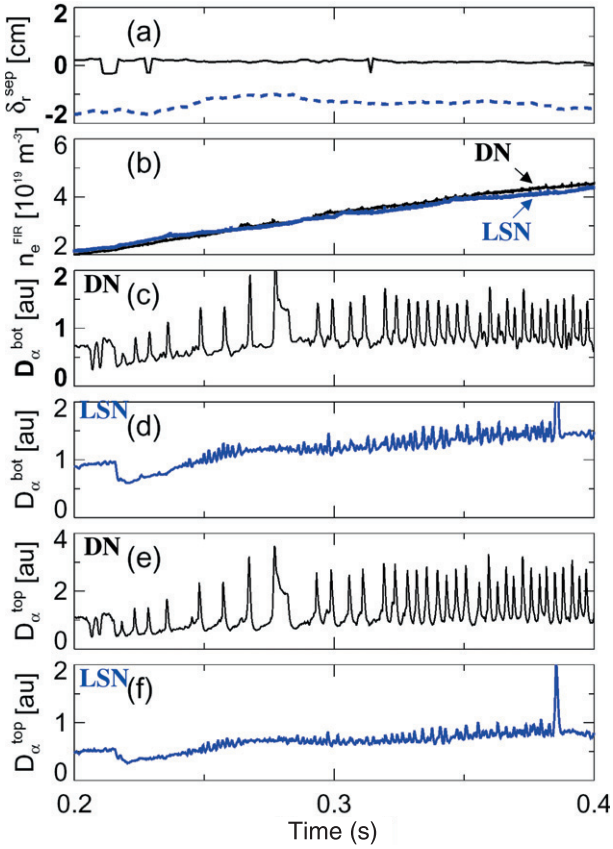

Figure 9. Effect of δ_r^{sep} variation on the ELM characteristics at $I_p = 0.8$ MA, $B_t = 0.45$ T, with $P_{NBI} = 4$ MW: (*a*) δ_r^{sep}, (*b*) $\overline{n_e}$, (*c*) lower divertor D_α for DN, (*d*) lower divertor D_α for LSN, (*e*) upper divertor D_α for DN and (*f*) upper divertor D_α for LSN.

5. Summary, discussion and conclusions

We have observed a high performance regime in NSTX, which is compatible with tiny ELMs with a frequency ~300–800 Hz. The stored energy drop per type V ELM is not statistically measurable, i.e. <1%. The perturbations are visible in the USXR diagnostic, which precedes the D_α burst in the divertor. There is no clear P_{NBI} scaling. The type V ELMs are observed with P_{NBI} up to 6.2 MW, and occasionally larger type I ELMs co-exist with these ELMs. There is a clear electromagnetic $n = 1$ precursor rotating counter to the plasma current before the type V ELM crash.

Type V ELMs show obvious differences compared with published ELM types, many of which have also been observed in other NSTX discharges. Some of the highest power NSTX discharges also have type I ELMs mixed in with type V ELMs, but type II/III ELMs are observed with different discharge

shapes. The NSTX type V ELMs are observed at medium to high density (between 0.5 and 1 X n_{GW}, with typical pedestal electron collisionality between 1 and 10). The compatibility of type V ELMs with high performance plasmas and the calculations showing that density control would be possible with active pumping make this operating regime an attractive possibility for next generation devices. Extrapolation of this regime to conventional aspect ratio tokamaks and a theoretical explanation of the instability mechanism are being explored.

Acknowledgments

This research was supported by the US Department of Energy under contracts DE-AC05-00OR22725, DE-AC02-76CH03073 and W-7405-ENG-36, and grants DE-FG02-99ER54519, DE-FG02-99ER54523 and DE-FG02-99ER54524. We gratefully acknowledge the contributions of the NSTX operations staff.

References

[1] ITER Physics Basis Authors 1999 *Nucl. Fusion* **39** 2137
[2] Loarte A. *et al* 2003 *J. Nucl. Mater.* **313–316** 962
[3] Federici G. *et al* 2003 *J. Nucl. Mater.* **313–316** 11
[4] Greenfield C.M. *et al* 2001 *Phys. Rev. Lett.* **86** 4544
[5] Takase Y. *et al* 1997 *Phys. Plasmas* **4** 1647
[6] Kaye S.M. *et al* 1984 *J. Nucl. Mater.* **121** 115
[7] Kamiya K. *et al* 2003 *Nucl. Fusion* **43** 1214
[8] Kamada Y. *et al* 2000 *Plasma Phys. Control. Fusion* **42** A247
[9] Kamada Y. *et al* 2002 *Plasma Phys. Control. Fusion* **44** A279
[10] Evans T.E. *et al* 2004 *Phys. Rev. Lett.* **92**, article #235003
[11] Doyle E.J. *et al* 1991 *Phys. Fluids* B **3** 2300
[12] Osborne T.H. *et al* 1997 *Proc. 24th European Conf. on Controlled Fusion and Plasma Physics (Berchtesgaden, Germany, 1997) (Petit-Lancy, Switzerland)* (EPS)
[13] Ono M. *et al* 2000 *Nucl. Fusion* **40** 557
[14] Kaye S.M. *et al* 1997 *Nucl. Fusion* **37** 1303
[15] Greenwald M. *et al* 1988 *Nucl. Fusion* **28** 2199
[16] Gates D.A. *et al* 2003 *Phys. Plasmas* **10** 1659
[17] Menard J.E. *et al* 2003 *Nucl. Fusion* **43** 330
[18] Maingi R. *et al* 2003 *Plasma Phys. Control. Fusion* **45** 657
[19] Sabbagh S.A. *et al* 2002 *Phys. Plasmas* **9** 2085
[20] Nishino N. *et al* 2002 *J. Plasma Fusion Res.* **78** 1278
[21] Kaye S.M. *et al* 2004 Progress towards high performance plasmas in the National Spherical Torus Experiment (NSTX) *Nucl. Fusion* submitted
[22] Maingi R. *et al* 2004 H-mode turbulence, power threshold, ELM, and pedestal studies in NSTX *Nucl. Fusion* submitted
[23] Maingi R. *et al* 2005 ELMs and the H-mode pedestal in NSTX *J. Nucl. Mater.* **337–339** 727
[24] Lao L.L. *et al* 1985 *Nucl. Fusion* **25** 1611
[25] Sabbagh S.A. *et al* 2001 *Nucl. Fusion* **41** 1601
[26] Ozeki T. *et al* 1990 *Nucl. Fusion* **30** 1425
[27] Stober J. *et al* 2001 *Nucl. Fusion* **41** 1123
[28] Stutman D. *et al* 2003 *Rev. Sci. Instrum.* **74** 1982
[29] Lasnier C.J. *et al* 1998 *Nucl. Fusion* **38** 1225
[30] Meyer H. *et al* 2004 *Plasma Phys. Control. Fusion* **46** A291
[31] Glasser A.H. *et al* 1997 *Bull. Am. Phys. Soc.* **42** 1848
[32] Mahdavi M.A. *et al* 1995 *J. Nucl. Mater.* **220–222** 13